Conservative Split-Explicit Time Integration Methods for the Compressible Nonhydrostatic Equations

J. B. KLEMP, W. C. SKAMAROCK, AND J. DUDHIA

National Center for Atmospheric Research, Boulder, Colorado*

(Manuscript received 29 August 2006, in final form 22 November 2006)

ABSTRACT

Historically, time-split schemes for numerically integrating the nonhydrostatic compressible equations of motion have not formally conserved mass and other first-order flux quantities. In this paper, split-explicit integration techniques are developed that numerically conserve these properties by integrating prognostic equations for conserved quantities represented in flux form. These procedures are presented for both terrain-following height and hydrostatic pressure (mass) vertical coordinates, two potentially attractive frameworks for which the equation sets and integration techniques differ significantly. For each set of equations, the linear dispersion equation for acoustic/gravity waves is derived and analyzed to determine which terms must be solved in the small (acoustic) time steps and how these terms are represented in the time integration to achieve stability. Efficient techniques for including numerical filters for acoustic and external modes are also presented. Simulations for several idealized test cases in both the height and mass coordinates are presented to demonstrate that these integration techniques appear robust over a wide range of scales, from subcloud to synoptic.

1. Introduction

In numerically integrating the compressible nonhydrostatic equations of motion for atmospheric applications, the presence of high-frequency acoustic modes can place significant constraints on the allowable time steps that will maintain computational stability. As a result, a variety of techniques have been developed to achieve computational efficiency in nonhydrostatic numerical models, including semi-implicit time integration, split-explicit time stepping, and the integration of filtered equations. In this paper we focus on split-explicit integration techniques for the compressible nonhydrostatic equations, and propose new procedures that are suitable for integrating these equations when cast in conservative (flux) form.

In semi-implicit schemes, the terms responsible for sound-wave propagation are averaged in time, producing an implicit set of equations for variables at the new time level that requires the solution of a three-dimensional Helmholz equation for pressure to complete each time step. Semi-implicit techniques have been developed for integrating the equations in Eulerian form (e.g., Tapp and White 1976) and have also frequently been employed in conjunction with a semi-Lagrangian integration (e.g., Tanguay et al. 1990; Staniforth and Côté 1991; Yeh et al. 2002). The semi-implicit semi-Lagrangian techniques add significant computational expense for each time step, and computational efficiency is often achieved by using larger time steps for which the Courant number may be significantly greater than unity. However, for nonhydrostatic and mesoscale applications, there is evidence that Courant numbers must remain less than unity in order to maintain desired accuracy in the simulations (e.g., Pinty et al. 1995; Bartello and Thomas 1996).

Another approach in solving the nonhydrostatic equations is to modify the equations to an anelastic form that does not admit acoustic modes. The anelastic equations were originally derived through scale analysis by Ogura and Phillips (1962), with modifications to improve their accuracy subsequently proposed by Wilhelmson and Ogura (1972), Lipps and Hemler (1982), and Durran (1989). With these techniques, the time derivative of density is ignored in the continuity equation and consequently pressure must be obtained each

* The National Center for Atmospheric Research is sponsored by the National Science Foundation.

Corresponding author address: Dr. Joseph B. Klemp, National Center for Atmospheric Research, P.O. Box 3000, Boulder, CO 80307-3000.
E-mail: klemp@ucar.edu

DOI: 10.1175/MWR3440.1

time step from the solution of a three-dimensional elliptic equation. Anelastic models have been successfully used in a wide variety of cloud and mesoscale applications (e.g., Clark 1977, 1979), and have been proposed as a framework for global applications (Smolarkiewicz et al. 2001), although the validity of these approximations for numerical weather prediction (NWP) or climate applications has been questioned (Davies et al. 2003).

With split-explicit techniques, the fully compressible nonhydrostatic equations can be integrated without the need to solve a three-dimensional elliptic equation. Computational efficiency is achieved by integrating the modes of physical interest with a time step appropriate for these modes, but then subdividing these time steps into a number of smaller (acoustic) time steps during which the terms responsible for sound-wave propagation are advanced in time (Klemp and Wilhelmson 1978). This approach was originally developed for cloud-scale modeling (Klemp and Wilhelmson 1978; Tripoli and Cotton 1982; Wicker and Wilhelmson 1995), and has subsequently been successfully adopted in a number of NWP models, such as the fifth-generation Pennsylvania State University–National Center for Atmospheric Research (NCAR) Mesoscale Model (MM5; Dudhia 1993), the Coupled Ocean/Atmosphere Mesoscale Prediction Systems (COAMPS; Hodur 1997), the Lokal Model (LM; Doms and Schättler 1999), the Advanced Regional Prediction System (ARPS; Xue et al. 2000), and the Japan Meteorological Agency nonhydrostatic model (JMA-NHM; Saito et al. 2006). Similar time-splitting techniques have been developed and analyzed for integrating the hydrostatic primitive equations (e.g., Madala 1981). The small time-step integration of acoustic terms can be viewed as an alternative solution procedure for the semi-implicit formulation; however it has the advantages that the numerical integration maintains the simplicity of the explicit time-stepping, high-frequency acoustic modes are not artificially retarded to lower frequencies comparable to modes of physical interest, and the split-explicit integration tends to be computationally more efficient than semi-implicit solvers for NWP applications (Thomas et al. 2000).

Historically, split-explicit integration schemes have not been designed to numerically conserve first-order quantities such as mass, momentum, and potential temperature coupled with density ($\rho\theta$). The equations have been cast in advective form and pressure is calculated from a prognostic equation of the general form

$$\partial_t p = -\frac{c^2}{\theta}(\nabla \cdot \rho\theta\mathbf{V} + \rho H_m), \tag{1}$$

derived by combining the continuity equation with the ideal gas law. Here, c is the speed of sound, and H_m represents diabatic contributions, principally from latent heating. With this approach density is computed diagnostically from the gas law, and thus mass will not be numerically conserved. Because the coefficient c^2 on the right-hand side of (1) is large, the primary effect in solving a prognostic pressure equation is to maintain the three-dimensional divergence near zero (which is rigorously enforced in the anelastic equations). Since the divergence term dominates in this equation, there is little restoring influence to keep the mean pressure from drifting (implying a corresponding mass drift) when incorporating open upper or lateral boundaries.

The pressure equation [(1)] has frequently been simplified for numerical convenience. One popular simplification has been to ignore the diabatic term in (1) (Klemp and Wilhelmson 1978; Dudhia 1993; Wicker and Wilhelmson 1995). Although testing this approximation appears to justify its use for many applications, the consequence of ignoring the diabatic term in the pressure equation is to effectively add an artificial source term to the continuity equation. In other words, diabatic heating does not directly increase the pressure because a compensating amount of mass is removed from the atmosphere. Dudhia (1993) has pointed out that this can have the beneficial effect of preventing artificial changes in pressure due to diabatic processes in models having a rigid-lid upper boundary.

Because of the dominant role of (1) in maintaining near nondivergence in the flow, this equation has also been viewed in the context of artificial compressibility (Chorin 1967), in which nondivergent flows are numerically integrated by solving a time dependent equation in the form of (1) with a large coefficient multiplying the divergence term to drive the solution to the desired state of nondivergence. This approach has been proposed for time-split integration schemes for the elastic equations, artificially decreasing the sound speed in (1) to increase the size of the small (acoustic) time steps (e.g., Droegemeier and Wilhelmson 1987; Tripoli 1992). However, combining this modified pressure equation with the gas law again reveals that the effective continuity equation has been altered with the addition of an artificial source/sink term for mass.

In this paper, we propose new split-explicit techniques for integrating the compressible nonhydrostatic equations that numerically conserve mass and other first-order conserved quantities. Using the flux form of the equations, we follow Ooyama's (1990) philosophy in formulating prognostic equations in terms of variables that have conservation properties and recover other variables (such as pressure and temperature)

from diagnostic relationships. In particular, we solve the full continuity equation as a prognostic equation, and ensure that the other flux-form equations are consistent with this equation (i.e., for a constant value of the scalar variable, the equation is numerically equivalent to the continuity equation). By ensuring mass conservation, this approach allows the conservation of other first-order flux quantities and eliminates the problem of pressure drift that can occur in time-split models in advective form that solve a prognostic pressure equation. Strict conservation of mass, moisture, and potential temperature is likely to be important for longer term integrations such as for regional climate and is also important for dynamical models used in atmospheric-chemistry and air-quality applications (Byun 1999).

In designing and testing conservative time-split techniques, we consider equation sets cast in terms of two different vertical coordinates that have potential application in cloud-scale and mesoscale models. Historically, cloud-scale models have utilized geometric height or terrain-following transformations based on height as the vertical coordinate. On the other hand, larger scale hydrostatic models typically employ a terrain-following pressure (sigma) coordinate. Laprise (1992) proposed a formulation for the nonhydrostatic equations in terms of a terrain-following hydrostatic pressure, which is equivalent to the sigma coordinate. Since the mass in the layers between adjacent coordinate surfaces is proportional to the increment in the vertical coordinate across the layer, this coordinate is often referred to as the mass coordinate. The nonhydrostatic equation set in the mass coordinate is somewhat more complex than in the height coordinate since the coordinate surfaces move with time and transformation metrics are therefore time dependent. All nonhydrostatic time-split models to date have been formulated using height for the vertical coordinate, so there is little experience in determining how or if time-splitting techniques will work with the mass coordinate.

In developing the techniques for time-split integration of the flux-form nonhydrostatic equations, we begin in section 2 with the equations cast in terms of the terrain-following height coordinate and then consider, in section 3, the corresponding time-split procedures for the equation set using the mass coordinate. For each vertical coordinate, we consider the modifications required to accommodate moist processes and appropriate filters to control acoustic and/or external modes that are not of physical interest. Linear analyses of the dispersion equation for both vertical coordinates are derived in the appendix to identify the terms that must be integrated on the acoustic time steps and how they should be represented in time. Selected test simulations are presented in section 4 to demonstrate that the time-split procedures in both the height and mass coordinates are robust over a wide range of scales and produce nearly equivalent results. Summary comments are included in section 5 with a brief assessment of additional factors that distinguish the two coordinate frameworks.

2. Time splitting with a terrain-following height coordinate

In writing the flux-form equations for the moist system, we choose to represent the flux variables in terms of the dry density ρ_d and to solve a continuity equation for dry density. We then predict the mixing ratios of all moist species, where the mixing ratio is defined as the mass of moist species per unit mass of dry air. We follow this approach because ρ_d is a conserved quantity that can be used to formulate flux-form equations for other conserved variables that do not contain additional terms accounting for sources and sinks of liquid water.

For the moist system it is also convenient to define a modified potential temperature variable $\theta_m = \theta(1 + a'q_v)$, where q_v is the mixing ratio of water vapor and $a' \equiv R_v/R_d \simeq 1.61$, with R_d and R_v being the gas constants for dry air and water vapor, respectively. Note that θ_m is different from virtual potential temperature θ_v, where the constant is $a \simeq 0.61$ instead of a'. The following equations clarify the relationship between θ_m and θ_v:

$$p = \rho_d R_d T + \rho_d q_v R_v T = \rho_d R_d \pi\theta\left(1 + \frac{R_v}{R_d} q_v\right)$$
$$\equiv \rho_d R_d \pi\theta_m \equiv \rho_d(1 + q_v) R_d \pi\theta_v. \tag{2}$$

In formulating the prognostic equations in terms of quantities that have conservation properties, we define flux variables that are adjusted to include terrain effects through transformation of the vertical coordinate. To incorporate a terrain transformation into the equations expressed using geometric height z as the vertical coordinate, we specify the terrain-following vertical coordinate as $\zeta = \zeta(x, y, z)$. Defining a transformation-adjusted dry density $\tilde{\rho}_d = \rho_d/\zeta_z$, the flux variables become

$$\mathbf{V} = \tilde{\rho}_d \mathbf{v} = (U, V, W), \quad \Theta_m = \tilde{\rho}_d \theta_m, \quad \text{and} \quad Q_j = \tilde{\rho}_d q_j, \tag{3}$$

where $q_j = (q_v, q_c, q_r, \ldots)$ includes the mixing ratios of cloud water q_c, rainwater q_r, and any other moist spe-

cies. The flux-form nonhydrostatic equations can then be expressed as

$$\partial_t \mathbf{V}_H = -(\boldsymbol{\nabla} \cdot \mathbf{v}\mathbf{V}_H)_\zeta - \frac{\rho_d}{\rho_m}[\boldsymbol{\nabla}_\zeta \tilde{p}' + \partial_\zeta(\boldsymbol{\zeta}_H \tilde{p}')] + \mathbf{F}_{V_H} \equiv \mathbf{R}_{V_H}, \tag{4}$$

$$\partial_t W = -(\boldsymbol{\nabla} \cdot \mathbf{v}W)_\zeta - \frac{\rho_d}{\rho_m}[\partial_\zeta(\zeta_z \tilde{p}') + g\tilde{\rho}'_m] + F_W \equiv R_W, \tag{5}$$

$$\partial_t \Theta_m = -(\boldsymbol{\nabla} \cdot \mathbf{v}\Theta_m)_\zeta + F_{\Theta_m} \equiv R_{\Theta_m}, \tag{6}$$

$$\partial_t \tilde{\rho}'_d = -(\boldsymbol{\nabla} \cdot \mathbf{V})_\zeta \equiv R_{\rho_d}, \quad \text{and} \tag{7}$$

$$\partial_t Q_j = -(\boldsymbol{\nabla} \cdot \mathbf{v}Q_j)_\zeta + F_{Q_j}, \tag{8}$$

where $\rho_m = \rho_d(1 + q_v + q_c + q_r + \cdots)$ is the total mass density and $\tilde{\rho}_m = \rho_m/\zeta_z$. The factor ρ_d/ρ_m in the pressure-gradient terms arises because dry density is used to define the flux-form velocities while the inverse density multiplying the pressure-gradient terms represents the total mass density.

In writing these equations, we follow the notation of Dutton (1976) in defining

$$(\boldsymbol{\nabla} \cdot \mathbf{V}b)_\zeta = (\mathbf{V} \cdot \boldsymbol{\nabla}b)_\zeta + b(\boldsymbol{\nabla} \cdot \mathbf{V})_\zeta = \boldsymbol{\nabla}_\zeta \cdot (\mathbf{V}b) + \partial_\zeta(\Omega b) \tag{9}$$

for any scalar variable b. Here, $\Omega = \mathbf{V} \cdot \boldsymbol{\nabla}\zeta$ is the component of the mass flux in the direction normal to the coordinate surface, where $\boldsymbol{\nabla}\zeta = (\zeta_x, \zeta_y, \zeta_z)$ represents the metrics of the transformation, and $\boldsymbol{\nabla}_\zeta$ refers to the divergence operator along a constant ζ surface. In addition, $\mathbf{V}_H = (U, V)$, $(\boldsymbol{\nabla} \cdot \mathbf{v}\mathbf{V}_H)_\zeta = [(\boldsymbol{\nabla} \cdot \mathbf{v}U)_\zeta, (\boldsymbol{\nabla} \cdot \mathbf{v}V)_\zeta]$, and $\boldsymbol{\zeta}_H = (\zeta_x, \zeta_y)$. The $R_{()}$ notation is introduced in (4)–(7) to represent right-hand side terms in the time-split equations that follow.

In (4)–(8), the terms denoted by $F_{()}$ contain the Coriolis and diffusion terms as well as diabatic effects and any parameterized physics that arise in a full atmospheric prediction model. Pressure is obtained from the diagnostic equation of state:

$$p = p_0\left(\frac{R_d\Theta_m}{p_0}\right)^\gamma, \tag{10}$$

and $\tilde{p} = (p/\zeta_z)$. Here, $\gamma = c_p/c_v = 1.4$ is the ratio of the heat capacities for dry air, and p_0 is a reference surface pressure.

We have employed the traditional approach of using a time-invariant reference state to recast the thermodynamic variables in the above equations. Perturbation variables are defined as deviations from a time-invariant hydrostatically balanced dry reference state such that $p = \bar{p}(z) + p'$, $\rho_d = \bar{\rho}_d(z) + \rho'_d$, $\rho_m = \bar{\rho}_d(z) + \rho'_m$, and $\Theta_m = \bar{\rho}_d(z)\bar{\theta}(z) + \Theta'_m$. This choice reduces the horizontal pressure-gradient-force errors associated with sloping coordinate surfaces and also greatly reduces the machine round-off error in computing small differences between the vertical pressure-gradient and buoyancy terms. The introduction of perturbation quantities is not essential in this formulation; their use is motivated by the desire for higher accuracy and greater flexibility in the choice of discretizations.

In contrast to most existing compressible nonhydrostatic models, by integrating (4)–(8), we do not integrate a prognostic pressure equation (typically an equation cast in terms of p or the Exner function π). Instead, (6) takes the place of a pressure equation. Since from (10) it is clear that pressure is just Θ_m raised to the power γ, (6) can be interpreted as a modified form of the pressure equation that has conservative properties. With this interpretation in mind, we can also use (10) to express the pressure-gradient terms in (4) and (5) in terms of Θ_m using the relation

$$\boldsymbol{\nabla}p = \gamma R_d \pi \boldsymbol{\nabla}\Theta_m,$$

where $\pi = (p/p_0)^\kappa$ and $\kappa = R_d/c_p$. The resulting unapproximated momentum equations are

$$\partial_t \mathbf{V}_H = -(\boldsymbol{\nabla} \cdot \mathbf{v}\mathbf{V}_H)_\zeta - \frac{\rho_d}{\rho_m}\gamma R_d \pi[\boldsymbol{\nabla}_\zeta \Theta'_m + \partial_\zeta(\boldsymbol{\zeta}_H \Theta'_m)] + \mathbf{F}_{V_H} \tag{11}$$

$$\partial_t W = -(\boldsymbol{\nabla} \cdot \mathbf{v}W)_\zeta - \frac{\rho_d}{\rho_m}\left[\gamma R_d \pi \partial_\zeta(\zeta_z \Theta'_m) - g\left(\tilde{\bar{\rho}}_d \frac{\pi'}{\bar{\pi}} - \tilde{\rho}'_m\right)\right] + F_W. \tag{12}$$

Since the presence of acoustic modes places a severe restriction on the time step, we utilize time splitting in the explicit numerical integration scheme to gain computational efficiency. The partitioning of terms between the large and small time steps, and the small time-step temporal discretization, are guided by an examination of the linear dispersion relation governing acoustic and gravity waves given in the appendix. Because gravity wave modes have significantly lower frequencies than the acoustic modes, they can, in principle, be evaluated on the large time steps in a split explicit scheme. Solving the prognostic equations in advective form, Klemp and Wilhelmsom (1978) evaluated the potential temperature equation and the buoyancy term in the vertical momentum equation on the large time steps for simulations of convective storms with horizontal grids of several kilometers or less. However, Skamarock and Klemp (1992) documented that for horizontal grids of several tens of kilometers or greater,

the buoyancy frequency may impose significant constraints on the size of the large time step, particularly in regions of high atmospheric stability. Consequently, here we also include terms fundamental to gravity wave propagation on the small time steps. Since the advection of Θ_m in (6) and the mass divergence term in the density equation [(7)] must both be integrated on the small time steps to maintain stability for the acoustic modes, the gravity wave modes are accommodated on the small time steps by simply including the buoyancy term in the vertical momentum equation [(5)] in the small time-step integration (at little computational expense), thereby removing the buoyancy–frequency limitation on the size of the large time steps (see appendix).

In evaluating terms on the small time steps, those containing horizontal derivatives are time integrated using forward–backward differencing, with forward differencing in the horizontal momentum equations and backward differencing in the potential temperature and density equations, which is analogous to the forward–backward scheme used by Klemp and Wilhelmson (1978). Since the vertical grid size is often much smaller than the horizontal grid length, the explicit treatment of terms responsible for the vertical propagation of acoustic modes could cause severe restrictions on the small time step. Therefore, these terms are solved implicitly on the small time steps to remove this limitation (see appendix).

To facilitate this small time-step integration, we recast the equations using prognostic variables expressed as perturbations from their values at time t by defining $\mathbf{V}'' = \mathbf{V} - \mathbf{V}^t = (U - U^t, V - V^t, W - W^t) = (U'', V'', W'')$, $\Theta''_m = \Theta_m - \Theta^t_m$, and $\tilde{\rho}''_d = \tilde{\rho}_d - \tilde{\rho}^t_d$, and noting that $\tilde{\rho}''_m = (\rho_m/\rho_d)\tilde{\rho}''_d$. Given these considerations, the temporally discrete form of the terms advanced during the acoustic time steps can be expressed as

$$\delta_\tau \mathbf{V}''_H + \frac{\rho^t_d}{\rho^t_m}\gamma R_d \pi^t [\nabla_\zeta \Theta''^{\tau}_m + \partial_\zeta(\boldsymbol{\zeta}_H \Theta''^{\tau}_m)] = \mathbf{R}^t_{V_H}, \tag{13}$$

$$\delta_\tau W'' + \frac{\rho^t_d}{\rho^t_m}\left[\gamma R_d \pi^t \partial_\zeta(\zeta_z \overline{\Theta''_m}^{\tau}) - g\tilde{\bar{\rho}}_d \frac{R_d}{c_v}\frac{\pi^t}{\bar{\pi}}\frac{\overline{\Theta''_m}^{\tau}}{\Theta^t_m}\right] + g\overline{\tilde{\rho}''_d}^{\tau} = R^t_W, \tag{14}$$

$$\delta_\tau \Theta''_m + \nabla_\zeta \cdot (\mathbf{V}''^{\tau+\Delta\tau}_H \theta^t_m) + \partial_\zeta(\overline{\Omega''}^{\tau}\theta^t_m) = R^t_{\Theta_m}, \quad \text{and} \tag{15}$$

$$\delta_\tau \tilde{\rho}''_d + \nabla_\zeta \cdot \mathbf{V}''^{\tau+\Delta\tau}_H + \partial_\zeta \overline{\Omega''}^{\tau} = R^t_{\rho_d}, \tag{16}$$

where $\Omega'' = \Omega - \Omega^t$, and the time-differencing and time-averaging operators are

$$\delta_\tau \phi = \frac{(\phi^{\tau+\Delta\tau} - \phi^{\tau})}{\Delta\tau} \quad \text{and}$$

$$\overline{\phi}^{\tau} = \frac{1+\beta_s}{2}\phi^{\tau+\Delta\tau} + \frac{1-\beta_s}{2}\phi^{\tau}. \tag{17}$$

The superscript t denotes the variables at time level t that are evaluated at the most recent large time step and held fixed during the acoustic time steps, and the right-hand sides $R^t_{(\,)}$ are defined in (4)–(7). To accommodate implicit treatment of the buoyancy term in (12) on the small time steps (see appendix), we have linearized the ideal gas law about the variables at time t to replace the π'' variable in the vertical momentum equation using $\pi'' = R_d \pi^t \Theta''_m/(c_v \Theta^t_m)$. This is the only approximation to the small-step equations, and it is highly accurate since the perturbations are limited to the variations that occur over a single large time step.

Representing the velocity variables as perturbations about the time level t is a new approach in solving the small-step equations, and it has the benefit of evaluating virtually all the slow-mode contributions to the flux divergence terms in (15) on the large time step. Thus, computationally expensive high-order or monotonic flux schemes only need to be used on the large time steps in the potential temperature equation [(15)]. If we evaluated the full flux divergence of Θ_m on the small time step, the cost of the flux schemes would be much higher because they would be computed on each acoustic time step, and they would be difficult to implement in the vertically implicit solution procedure.

Integrating over a small time step $\Delta\tau$, the horizontal momentum equations [(13)] are integrated first, with terms involving Θ''_m evaluated at time τ. Next, (14)–(16) are integrated, using $\mathbf{V}''^{\tau+\Delta\tau}_H$ for the horizontal gradient terms in (15)–(16). Equations (14)–(16), however, are implicitly coupled in the vertical. To form a vertically implicit equation for Ω'', the relationship $\Omega'' = \zeta_x U'' + \zeta_y V'' + \zeta_z W''$ is used to write $\delta_\tau W''$ in (14) in terms of $\delta_\tau \Omega''$, given that $\zeta_x \delta_\tau U'' + \zeta_y \delta_\tau V''$ can be evaluated using the updated horizontal velocities. [With second-order vertical differencing on a C grid, eliminating $\tilde{\rho}''_d$ and Θ''_m from (14) using (15) and (16) results in a tridiagonal equation for Ω'' that is easily inverted.] Having solved (14), (15) and (16) are then evaluated.

Within the acoustic time steps, the prognostic variables for the discrete equations are U'', V'', Ω'', Θ''_m, and $\tilde{\rho}''_d$, and the coefficients multiplying terms involving these variables are evaluated at time t and held fixed during the small time steps. Neither the Exner function π, nor the vertical velocity W, nor the uncoupled variables θ_m and $\mathbf{v}$ need evaluation during the small time steps. The upper and lower boundary conditions are

also cast in terms of these variables (i.e., $\Omega'' = 0$ at the surface and at the upper lid). Thus, the time-splitting procedures involve only the dynamical equations [(13)–(16)] on the small time steps. The moisture equations [(8)] and any other scalar transport variables in the model system can be represented in flux form and integrated on the large time steps using velocities in the flux divergence terms that have been averaged in time over the small time steps to insure conservation.

a. Treatment of diabatic forcing

Diabatic influences H_m in the Θ_m equation [(15)] are contained in $R^t_{\Theta_m}$, and have the form

$$H_m = (1 + a' q_v) M_\theta + a' M_{q_v}, \tag{18}$$

where M_θ and M_{q_v} represent the diabatic contributions to $d\theta/dt$ and dq_v/dt, respectively. In addition, the moisture equations [(8)] contain microphysical and sedimentation terms M_{q_j} that are a part of F_{Q_j}. Although the microphysical effects H_m and M_{q_j} are computed on the large time steps, these influences are typically omitted from $R^t_{\Theta_m}$ in (15) and then included as adjustments to the potential temperature and moisture variables after both the variables have been advanced to the new time level. This approach is adopted in most time-split models to enable saturated conditions to be exactly satisfied by variables at the new time level. We have found, however, that this procedure can introduce some noise in the time-split integration, analogous to that encountered with additive splitting techniques [see Skamarock and Klemp (1992) and references therein]. To effectively remove this source of noise, we have refined the conventional time-split procedure by including an estimate of H_m as part of $R^t_{\Theta_m}$ in (15) for the acoustic substeps using a value that is retained from the previous time step, and then correcting the microphysical adjustment at the end of the time step. Other physics tendencies as well as diffusive and advective terms are known prior to computing the small time steps and can be accurately represented on the right-hand sides of the equations advanced on the acoustic steps.

b. Acoustic-mode filtering

Stability analyses of time-split integration schemes have documented the need for acoustic filtering to insure numerical stability over a wide range of applications (Skamarock and Klemp 1992; Wicker and Skamarock 1998). This filtering can be accomplished by forward centering the vertically implicit portion of the small time steps (Durran and Klemp 1983) and/or by adding a 3D divergence damping term to the horizontal momentum equations (Skamarock and Klemp 1992). Forward centering of the vertically implicit terms in (13)–(16) is accomplished by defining the time-averaging operator as indicated in (17), with a coefficient typically $\beta_s = 0.1$.

To more selectively damp acoustic modes, Skamarock and Klemp (1992) proposed adding a term to each of momentum equations that is proportional to the gradient of the 3D divergence. These terms have the effect of introducing a second-order diffusion of the 3D divergence, which is highly specific to filtering acoustic modes. For the current time-split integration scheme, we propose a modified version of divergence damping that is implemented by simply replacing Θ''^{τ}_m in the pressure-gradient terms in the horizontal momentum equation with a modified value:

$$\Theta''^{*}_m = \Theta''^{\tau}_m + \beta_d (\Theta''^{\tau}_m - \Theta''^{\tau-\Delta\tau}_m), \tag{19}$$

where β_d is the divergence damping coefficient (typically set to $\beta_d = 0.1$). With this representation, the horizontal pressure-gradient terms are slightly forward centered from the time level τ that is used in the forward backward differencing of the horizontal gradient terms in (13)–(16). This off-centering will damp high-frequency horizontally propagating modes in a manner similar to the off-centering of the vertically implicit term that damps high frequency vertically propagating modes. This horizontal filter, however, is more selective to acoustic modes since it is essentially equivalent to damping the 3D divergence as proposed by Skamarock and Klemp (1992). Instead of adding a term proportional the horizontal gradient of the 3D divergence, (19) corresponds to adding a term proportional to the horizontal gradient of $\delta_\tau \Theta_m \simeq -\nabla \cdot (\Theta_m \mathbf{v}) + \rho_d H_m$. Damping this expression is consistent with an equation of anelastic balance given by $\nabla \cdot (\rho_d \theta_m \mathbf{v}) = \rho_d H_m$, which was proposed by Durran (1989) as an improved representation of the anelastic approximation. (This expression is actually a modification of Durran's expression that results from including moisture in the gas law.) Implementing the divergence damping using (19) instead of constructing the full 3D divergence also significantly streamlines the required computations.

3. Time splitting with a terrain-following hydrostatic pressure coordinate

Laprise (1992) introduced an equation set for the compressible nonhydrostatic equations in terms of a terrain-following hydrostatic pressure vertical coordinate

$$\eta = (p_h - p_{ht})/\mu_d, \tag{20}$$

where $\mu = p_{hs} - p_{ht}$, p_h is the hydrostatic component of the pressure for dry air, and p_{hs} and p_{ht} refer to values along the surface and top boundaries, respectively. Here, we recast Laprise's equations in flux form to achieve conservation for the prognostic variables. While this approach is analogous to those used in some hydrostatic models (e.g., Anthes and Warner 1978), it is unique for nonhydrostatic models in this coordinate. Since $\mu_d(x, y)$ represents the mass of dry air per unit area within the column in the model domain at (x, y), the appropriate flux-form variables become

$$\mathbf{V} = \mu_d \mathbf{v} = (U, V, W),\ \Omega = \mu_d \dot{\eta},\ \Theta = \mu_d \theta, \quad \text{and}$$
$$Q_j = \mu_d q_j. \tag{21}$$

As with the height-coordinate formulation, we define flux variables in terms of dry air to avoid the appearance of source and sink terms for condensed water in the flux-form equations. Using these variables, we again follow Ooyama's (1990) approach in writing the prognostic equations in terms of variables that have conservation properties and recast Laprise's (1992) equations in flux form for a moist atmosphere:

$$\partial_t \mathbf{V}_H = -(\nabla \cdot \mathbf{v}\mathbf{V}_H)_\eta - \mu_d \frac{\alpha_m}{\alpha_d}\left(\alpha_d \nabla_\eta p + \frac{1}{\mu_d}\partial_\eta p \nabla_\eta \phi\right) + \mathbf{F}_{V_H} \equiv \mathbf{R}_{V_H}, \tag{22}$$

$$\partial_t W = -(\nabla \cdot \mathbf{v}W)_\eta + g\left(\frac{\alpha_m}{\alpha_d}\partial_\eta p - \mu_d\right) + F_W \equiv R_W, \tag{23}$$

$$\partial_t \Theta = -(\nabla \cdot \mathbf{v}\Theta)_\eta + F_\Theta \equiv R_\Theta, \tag{24}$$

$$\partial_t \phi = -(\mathbf{v} \cdot \nabla \phi)_\eta + gw \equiv R_\phi, \tag{25}$$

$$\partial_t \mu_d = -(\nabla \cdot \mathbf{V})_\eta, \quad \text{and} \tag{26}$$

$$\partial_t Q_j = -(\nabla \cdot \mathbf{v}Q_j)_\eta + F_{Q_j}, \tag{27}$$

together with diagnostic relations for the hydrostatic pressure

$$\partial_\eta \phi = -\mu_d \alpha_d \tag{28}$$

and the gas law

$$p = \left(\frac{R_d \theta_m}{p_0 \alpha_d}\right)^\gamma. \tag{29}$$

The specific volume $\alpha_m = \alpha_d(1 + q_v + q_c + q_r + \cdots)^{-1}$ for a moist environment, whereas $\alpha_m = \alpha_d$ and $\theta_m = \theta$ for dry air. Here, the prognostic equation [(25)] for geopotential $\phi \equiv gz$ is an exception to the approach of writing the prognostic equations in terms of conserved variables, since geopotential is not a conserved quantity and its equation represents the definition of vertical velocity ($dz/dt \equiv w$). As pointed out by Laprise (1992), the nonhydrostatic equation set in the mass coordinate can be solved using either a prognostic equation for pressure or a prognostic equation for the geopotential. We have chosen the latter approach as it is computationally simpler (it avoids computing the full 3D divergence), and removes the potential for pressure drift discussed in the previous section.

For this system of equations, it is also desirable to reduce truncation errors in the finite differencing by defining variables as perturbations from a hydrostatically balanced reference state. For this purpose, we define reference variables (denoted by overbars) that are a function of height only and that satisfy (22)–(29) for an atmosphere at rest. In this manner, $p = \bar{p}(\bar{z}) + p'$, $\phi = \bar{\phi}(\bar{z}) + \phi'$, $\alpha = \bar{\alpha}(\bar{z}) + \alpha'$, and $\mu_d = \bar{\mu}_d(x) + \mu'_d$. Because the η coordinate surfaces are generally not horizontal, the reference profiles $\bar{p}$, $\bar{\phi}$, and $\bar{\alpha}$ are functions of (x, y, η). Notice also that the reference variables are defined in terms of the height $\bar{z}$ in the reference sounding, and therefore do not change in time at model grid points even though the coordinate surfaces move vertically over time. Using these perturbation variables, the hydrostatically balanced portion of the pressure gradients in the reference sounding can be removed without approximation in the equations, such that the momentum equations [(22) and (23)] become

$$\mathbf{R}_{V_H} = -(\nabla \cdot \mathbf{v}\mathbf{V}_H)_\eta - \mu_d \frac{\alpha_m}{\alpha_d}\left[\alpha_d \nabla_\eta p' + (\nabla_\eta \bar{p})\alpha'_d + \nabla_\eta \phi' + \frac{1}{\mu_d}(\nabla_\eta \phi)(\partial_\eta p' - \mu'_d)\right] + \mathbf{F}_{V_H} \quad \text{and} \tag{30}$$

$$R_W = -(\nabla \cdot \mathbf{v}W)_\eta + g\left(\frac{\alpha_m}{\alpha_d}\partial_\eta p' - \mu'_d + \bar{\mu}_d \frac{\alpha - \alpha_d}{\alpha_d}\right) + F_W, \tag{31}$$

and similarly (28) becomes

$$\partial_\eta \phi' = -\bar{\mu}_d \alpha'_d - \alpha_d \mu'_d. \tag{32}$$

In constructing a split-explicit time integration scheme for the mass-coordinate equations, we again identify the terms that are fundamentally responsible for acoustic and gravity wave propagation and evaluate these terms on smaller acoustic time steps (see appendix), while the remaining terms (advection, diffusion, Coriolis, parameterized physics, etc.) are updated on larger time steps appropriate for the modes of physical interest. With this approach, constraints on the size of

the large time step due to the speed of sound and the buoyancy frequency are again removed.

To facilitate the integration of these equations over the small acoustic time steps in the time-split scheme, we again define small time-step variables that represent deviations from the most recent large time-step values (denoted by superscript t):

$$\mathbf{V}'' = \mathbf{V} - \mathbf{V}^t, \quad \Omega'' = \Omega - \Omega^t, \quad \Theta'' = \Theta - \Theta^t,$$

$$\phi'' = \phi' - \phi'^t, \quad p'' = p' - p'^t, \quad \alpha'' = \alpha' - \alpha'^t, \quad \text{and}$$

$$\mu_d'' = \mu_d' - \mu_d'^t. \tag{33}$$

Using these variables, the equations integrated over the small time steps $\Delta\tau$ take the form

$$\delta_\tau \mathbf{V}''_H + \mu_d^t \frac{\alpha_m^t}{\alpha_d^t}\left[\alpha_d^t \nabla_\eta p''^\tau + (\nabla_\eta \overline{p})\alpha_d''^\tau + \nabla_\eta \phi''^\tau + \frac{1}{\mu_d^t}(\nabla_\eta \phi^t)(\partial_\eta p'' - \mu_d'')^\tau\right] = \mathbf{R}_{V_H}^t, \tag{34}$$

$$\delta_\tau \mu_d'' + [\nabla \cdot (\mathbf{V}''^{\tau+\Delta\tau} + \mathbf{V}^t)]_\eta = 0, \tag{35}$$

$$\delta_\tau \Theta'' + (\nabla \cdot \mathbf{V}''^{\tau+\Delta\tau}\theta^t)_\eta = R_\Theta^t, \tag{36}$$

$$\delta_\tau W'' - g\overline{\left(\frac{\alpha_m^t}{\alpha_d^t}\partial_\eta p'' - \mu_d''\right)}^\tau = R_W^t, \quad \text{and} \tag{37}$$

$$\partial_\tau \phi'' + \frac{1}{\mu_d^t}[(\mathbf{V}''^{\tau+\Delta\tau} \cdot \nabla \phi^t)_\eta - g\overline{W''}^\tau] = R_\phi^t, \tag{38}$$

where all of the terms represented by $R_{(\,)}^t$ on the right-hand sides of (34)–(38) are evaluated at time level t. In the thermodynamic equation [(36)] the diabatic terms H_m contained in R_Θ^t are initially estimated at time t and then corrected after completing the small time steps as discussed in section (2.1). As in the height-coordinate system, the moisture equations [(27)] and any other scalar equations are integrated on the large time steps.

For the small time-step integration, the expressions for perturbation pressure and specific density are derived from (29) and (32):

$$p'' = \frac{c^2}{\alpha_d^t}\left(\frac{\Theta''}{\Theta^t} - \frac{\alpha_d''}{\alpha_d^t} - \frac{\mu_d''}{\mu_d^t}\right) \quad \text{and} \tag{39}$$

$$\alpha_d'' = -\frac{1}{\mu_d^t}(\partial_\eta \phi'' + \alpha_d^t \mu_d''), \tag{40}$$

where $c^2 = \gamma p^t \alpha_d^t$ is the square of the sound speed.

The expression (39) for p'' is obtained by linearizing the gas law (29) about the most recent large time-step values. This increases the efficiency on the small steps by eliminating the exponentiation, but more importantly, allows the vertical pressure gradient in (37) to be expressed in terms of ϕ'' in order to solve implicitly for the vertically propagating acoustic modes. Combining (39) and (40), the vertical pressure gradient $\partial_\eta p''$ can be expressed as

$$\partial_\eta p'' = \partial_\eta\left(\frac{c^2}{\mu_d^t \alpha_d^{t2}}\partial_\eta \phi''\right) + \partial_\eta\left(\frac{c^2}{\alpha_d^t}\frac{\Theta''}{\Theta^t}\right). \tag{41}$$

This linearization about the most recent large time step should be highly accurate over the time interval of the several small time steps.

The integration over the small time steps proceeds in the following manner: Starting with all of the small time-step variables at time τ, (34) is stepped forward to obtain $U''^{\tau+\Delta\tau}$ and $V''^{\tau+\Delta\tau}$. Both $\mu_d''^{\tau+\Delta\tau}$ and $\Omega''^{\tau+\Delta\tau}$ are then calculated from (35). This is accomplished by first integrating (35) vertically from the surface to the material surface at the top of the domain, which removes the $\partial_\eta\Omega$ term such that

$$\delta_\tau \mu_d'' = \int_1^0 \nabla_\eta \cdot (\mathbf{V}''^{\tau+\Delta\tau} + \mathbf{V}^t)\, d\eta. \tag{42}$$

After computing $\mu_d''^{\tau+\Delta\tau}$ from (42), $\Omega''^{\tau+\Delta\tau}$ is recovered by integrating the $\partial_\eta\Omega''$ term in (35) vertically, using the boundary condition $\Omega'' = 0$ at the surface. Equation (36) is then stepped forward to calculate $\Theta''^{\tau+\Delta\tau}$. Equations (37) and (38) are combined using (41) to form a vertically implicit equation that is solved for $W''^{\tau+\Delta\tau}$ subject to the boundary conditions $W'' = \mathbf{V}'' \cdot \nabla h$ at the surface $z = h(x, y)$, and a specification for p' or W along the upper boundary of the domain. Then $\phi''^{\tau+\Delta\tau}$ is obtained from (38), and $p''^{\tau+\Delta\tau}$ and $\alpha_d''^{\tau+\Delta\tau}$ are recovered from (39) and (40), respectively.

a. Hydrostatic option

Writing the nonhydrostatic equations using hydrostatic pressure as the vertical coordinate allows solutions to the corresponding hydrostatic equations to be generated with only small modifications to the full nonhydrostatic code. To compute the hydrostatic solution, the integration procedure steps forward (34)–(36) as described above for the nonhydrostatic system. Next, instead of solving prognostic equations (37) and (38), the hydrostatic equation $\partial_\eta p'' = (\alpha_d/\alpha)^t \mu_d''$ is integrated vertically to obtain $p''^{\tau+\Delta\tau}$, $\alpha_d''^{\tau+\Delta\tau}$ is diagnosed from the gas law (39), and $\phi''^{\tau+\Delta\tau}$ is recovered through vertical integration of (40), in that order. On the large time steps, the full perturbation pressure is computed from the hydrostatic equation

$$\partial_\eta p' = \frac{\alpha_d}{\alpha}\mu_d - \overline{\mu}_d. \tag{43}$$

Thus, by employing a few simple switches in the code, either nonhydrostatic or hydrostatic solutions can be produced for the governing equations.

For large-scale hydrostatic-flow applications, utilizing the hydrostatic option improves the numerical efficiency by avoiding the computationally more expensive vertically implicit solution of (37), (38), and (41), although the nonhydrostatic integration will produce essentially the same result. In the hydrostatic system, the vertical velocity does not appear in the equations, and vertical motion is represented by Ω. Further computational efficiency can be gained in the hydrostatic option by writing the perturbation form of the hydrostatic pressure-gradient terms in the horizontal momentum equations in terms of α instead of α_d:

$$\alpha\boldsymbol{\nabla}_z p = \alpha\boldsymbol{\nabla}_\eta p + \boldsymbol{\nabla}_\eta\phi = \alpha\boldsymbol{\nabla}_\eta p' + \alpha'\boldsymbol{\nabla}_\eta\bar{p} + \boldsymbol{\nabla}_\eta\phi', \tag{44}$$

which allows the cancellation of several terms in the full pressure gradient through the hydrostatic equation [(43)].

b. Acoustic-mode filtering

Filtering for the acoustic modes in the mass-coordinate equations is accomplished in a similar manner to techniques used for the height-coordinate system. The time averaging in the vertically implicit portion of the small time steps in (34)–(38) can be slightly forward centered using the averaging operator defined in (17). In addition, terms can be added to the horizontal momentum equations that specifically damp the 3D divergence. Here, we again represent the 3D divergence in terms of the time derivative of the pressure and employ a modified pressure in the horizontal pressure-gradient terms in (34) that adjusts the pressure slightly forward in time. Since these gradient terms are expressed in terms of p'' instead of Θ_m'' as in (19), we replace p''^{τ} by

$$p''^{*} = p''^{\tau} + \beta_d(p''^{\tau} - p''^{\tau-\Delta\tau}) \tag{45}$$

on the left-hand side of (34). Although we do not solve a prognostic equation for pressure, this equation is readily derived by logarithmically differentiating (29) with respect to time as in (1), yielding

$$\delta_\tau p'' \simeq -\frac{c^2}{\theta_m}[\boldsymbol{\nabla}\cdot(\rho_d\theta_m\mathbf{v}) - \rho_d H_m].$$

Thus, adding a small portion of $\delta_\tau p''$ into the horizontal pressure-gradient terms is again consistent with damping toward Durran's (1989) anelastic balance, $\boldsymbol{\nabla}\cdot(\rho_d\theta_m\mathbf{v}) = \rho_d H_m$.

c. Upper boundary condition and external-mode filtering

To maintain control over the conservation of mass and other first-order quantities, it is highly beneficial to specify the upper boundary of the integration domain to be a material surface, such that $\Omega = 0$. Subject to this constraint, several different physical boundary conditions can be readily implemented. Solving the tridiagonal matrix resulting from the implicit equations [(37), (38), and (41)] requires an upper boundary condition for pressure or vertical velocity (or a relation between the two) in addition to the lower boundary condition provided by the surface terrain. Specifying $w = 0$ at the top will produce a rigid lid, while $p' = 0$ corresponds to a free (constant pressure) surface. A radiation condition for gravity waves can be imposed in a manner proposed by Klemp and Durran (1983) by Fourier transforming the vertical velocity along the upper boundary, applying a radiation condition to the Fourier modes, and then taking the inverse transform to recover the pressure along the upper boundary. (This can be accomplished as part of the implicit solver by applying the radiation condition at the top after removing the lower diagonal from the tridiagonal matrix.)

By relaxing the rigid lid constraint for the upper boundary, external modes can form that may be artificially excited. To control these modes, we have designed a new filter that is highly specific to external waves. This filter is similar in concept to the 3D divergence except that it damps the vertical integral of the horizontal divergence D_h, which contributes fundamentally to the existence of the external modes (analogous to the horizontal divergence in the shallow-water equations). To provide a filter for D_h, we add a term to the right-hand sides of the horizontal momentum equations of the form

$$\partial_t\mathbf{V}_H = \cdots - \gamma_e\boldsymbol{\nabla}_\eta(\partial_t\mu_d). \tag{46}$$

Here, $\partial_t\mu_d = D_h$, which is evident by vertically integrating the hydrostatic continuity equation as indicated in (42). By taking the horizontal divergence of (46) and then integrating all terms in the equation vertically with respect to η, we obtain

$$\partial_t D_h = \cdots + \gamma_e\boldsymbol{\nabla}_\eta^2 D_h, \tag{47}$$

which confirms that the term added to (46) results in the second-order diffusion of D_h. This filter is implemented in the small time-step integration by adding a term to the left-hand side of (34) of the form

$$\delta_\tau\mathbf{V}_H'' + \cdots + \left(\frac{\beta_e\Delta h^2}{\Delta\tau}\right)\boldsymbol{\nabla}_\eta(\delta_{\tau-\Delta\tau}\mu_d'') = \mathbf{R}_{V_H}, \tag{48}$$

where $\Delta h = \Delta x = \Delta y$, and $\beta_e = \gamma_e \Delta\tau/\Delta h^2$ is the dimensionless filter coefficient that is typically set to $\beta_e = 0.01$. Notice that this filter term does not depend on height and therefore only needs to be computed once for each vertical column.

4. Model numerics and sample applications

The techniques described above for time splitting of the nonhydrostatic equations expressed in flux form do not require the specification of any particular spatial differencing, time differencing on the large time steps, or grid staggering. These choices can be made based on user preferences and requirements for the intended range of model applications.

In considering the large time-step integration techniques, stable schemes for time-split models have been demonstrated using leapfrog (Klemp and Wilhelmson 1978; Skamarock and Klemp 1992), second-order Runge–Kutta (Wicker and Skamarock 1998), and third-order Runge–Kutta (Wicker and Skamarock 2002) time integration. The leapfrog scheme is the simplest to implement; its detracting factors are that it is a three time level scheme and small time steps must be integrated over a time interval of $2\Delta t$ for each large time step, it is only stable for centered (even order) advection, and it is technically only first-order accurate in time because of the required time smoothing. The second-order Runge–Kutta is a forward-in-time scheme in which the advection terms must be computed twice for each large time step. It is stable only for upwind (odd-order) differencing of the advection terms and the allowable time step is significantly restricted when using the higher order advection schemes (Wicker and Skamarock 1998). The third-order Runge–Kutta time integration is stable for both centered and upwind differencing for advection and allows a stable time step that is about twice the value that can be used in leapfrog (Wicker and Skamarock 2002). It is third order in time (formally for linear disturbances) and requires three computations of the advection terms for each time step.

For the staggering of variables on the computational grid, we have chosen the Arakawa C grid as it provides the best resolution of gravity waves (Arakawa and Lamb 1977); these are the most important modes near the grid scale in nonhydrostatic applications, which is where selectively higher numerical resolution is most needed. On the C grid, the pressure-gradient and divergence terms are computed over a single grid interval. Using second-order spatial differences for these terms thus provides accuracy comparable to fourth-order differencing on an unstaggered grid for waves of intermediate resolution, and provides significantly greater accuracy at high wavenumbers (e.g., Durran 1999, p. 115), although the convergence of low wavenumber modes with increasing resolution remains second order.

To test and evaluate the time-splitting techniques presented here, we originally developed 2D prototype codes for both the terrain-following height and mass vertical coordinates using, for simplicity, leapfrog differencing for the large time steps and second-order centered representations for all required spatial averaging and differencing. With these codes we have conducted simulations for a variety of idealized test cases such as density currents, mountain waves, and 2D squall lines across a range of horizontal scales (Δx ranging from 100 m to 20 km). These simulations confirm that the proposed time-splitting procedures for the flux-form equations are robust across a broad range of scales, that the height- and mass-based coordinates produce virtually identical results, and that mass is conserved in the simulations to machine accuracy.

To illustrate these results, we present here the simulation for the 2D density current. This simulation follows the benchmark case analyzed by Straka et al. (1993). A density current is generated within a neutrally stable atmosphere by a cold bubble that descends to the surface and then spreads out laterally due to the negative buoyancy of the cold air. The parameters are defined as specified by Straka et al. Using a constant diffusion coefficient ($75\ m^2\ s^{-1}$) the numerical solutions will converge in the limit of small grid increments. For this test, we have specified $\Delta x = \Delta z \simeq 100$ m, and integrate the time-split equations with a large time step $\Delta t = 1$ s and small time step $\Delta\tau = 0.25$ s. The evolving density current is displayed in Fig. 1 for both the height- and mass-coordinate simulations. The two simulations are nearly identical and both agree well with the reference results presented by Straka et al.

Based on the successful testing of the 2D implementations, we developed 3D versions of the conservative equations in both height and mass coordinates. For the numerics, we adopted the time-split third-order Runge–Kutta time integration scheme (Wicker and Skamarock 2002) along with flux-form advection operators selectable from second to sixth order (fifth-order upwind advection is used for the test cases described below). By including a full suite of physics packages and procedures to initialize the model with real data, these constituted the early prototypes for the Weather Researching and Forecasting (WRF) model (Skamarock et al. 2001, 2005). Testing these 3D implementations in a variety of idealized applications provides further confirmation of the robust nature of these

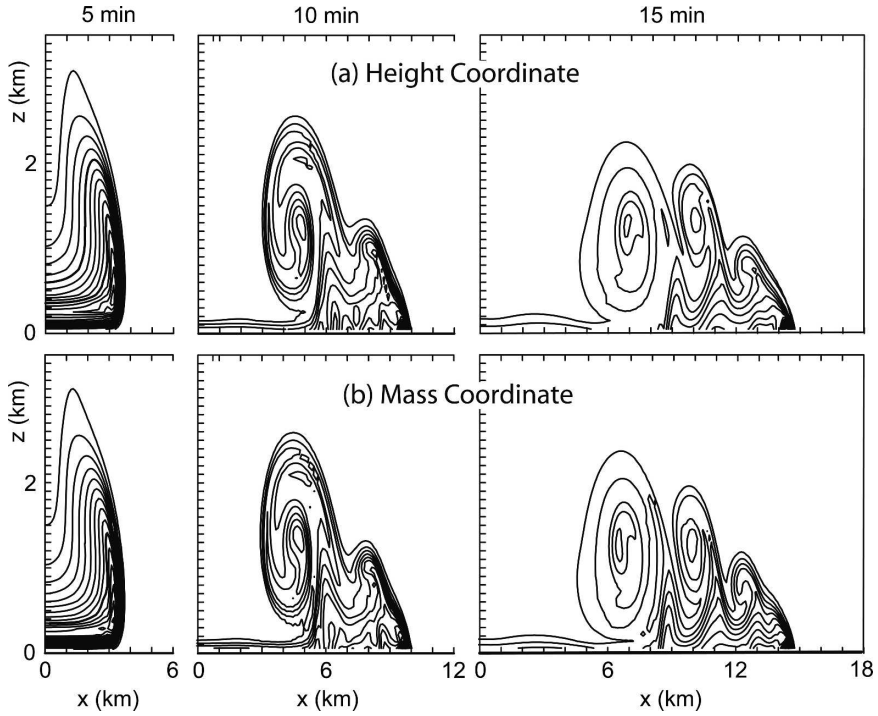

FIG. 1. Potential temperature field for Straka et al. (1993) 2D density-current benchmark case for (a) height-coordinate and (b) mass-coordinate simulations for $\Delta x = \Delta z \simeq 100$ m. Contour interval (CI) is 1 K.

time-split techniques for integrating the nonhydrostatic flux-form equations.

The simulation of an idealized supercell thunderstorm, depicted in Fig. 2, illustrates the ability of these codes to model strong convective systems, which provides a stringent test for model numerics since moist instability provides significant forcing (latent heating) near the grid scale. The sounding used for this simulation corresponds to case C presented by Weisman and Klemp (1984) for a splitting supercell with a stronger right-flank storm due to a quarter-circle turning of the wind shear between the surface and 2.5 km. The storm was simulated in an $80 \times 80 \times 20$ km domain with $\Delta x = \Delta y = 1$ km, $\Delta z \simeq 500$ m, and using a large time step $\Delta t = 6$ s and a small time step $\Delta\tau = 1.5$ s. Figure 2 displays the splitting supercell at 2 h for the simulation with the mass coordinate, which is virtually the same as the height-coordinate simulation (not shown). At this time, the storm has split into mature right- and left-moving storms with merging anvil outflow aloft. Although there is no absolute reference solution for this case, these results are quite similar to those produced with other cloud models.

To test these numerical techniques at very large scales, we have simulated the growth of an idealized moist baroclinic wave in a channel. The initialization for this case follows that described in Rotunno et al. (1994) except that, instead of a Boussinesq atmosphere, we invert the PV equation for the compressible atmosphere to obtain the initial 2D (y, z) jet structure. The maximum wind speeds in the initial jet are slightly less than 70 m s^{-1}. The domain is a periodic (west–east) channel of length 4000 km and width 8000 km. The north and south lateral boundaries are free-slip walls, and the lower boundary is also free slip. The domain height is approximately 16 km with an upper boundary that is a rigid lid for the height coordinate and a constant pressure surface for the mass coordinate. The grid intervals are set at $\Delta x = \Delta y = 100$ km, $\Delta z \simeq 250$ m, and the equations are integrated using $\Delta t = 10$ min, and $\Delta\tau = 2.5$ min. A small-amplitude, large-scale perturbation in the temperature field is imposed on the initial jet, from which the most unstable mode (the normal mode) grows and begins to dominate after about a day. The finite-amplitude disturbances are displayed in Fig. 3 at a time 3.5 days after the growing disturbance has reached an amplitude (defined as the maximum meridional velocity at $z = 150$ m) of 1 m s^{-1} in each simulation. At this time the two simulations exhibit nearly the same amplitude (slightly greater than 50 m s^{-1}), and Fig. 3 confirms that the structures of the breaking baroclinic waves are also very similar.

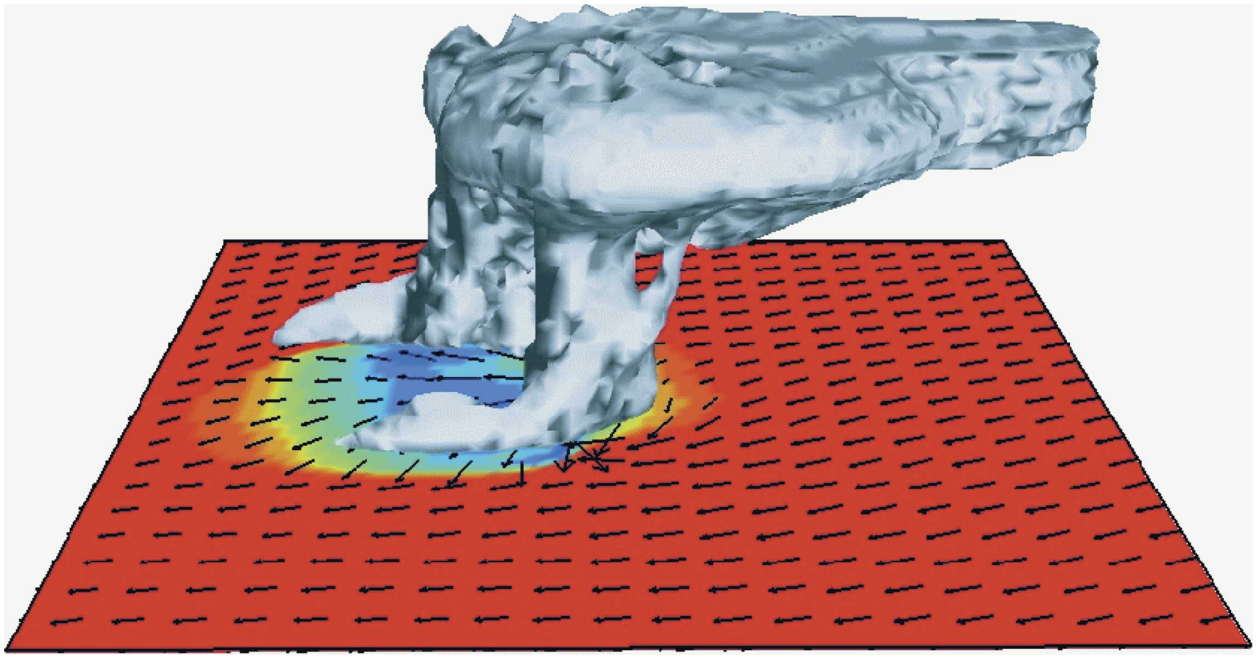

FIG. 2. Simulated splitting supercell thunderstorms evolving in strong environmental wind shear, displayed at 2 h. The cloud field is shaded in gray, surface temperature is colored in shades ranging from red (warm) to blue (cold), and surface wind vectors are included at every fourth interval. The model integration employed $\Delta x = \Delta y = 1$ km, $\Delta z \simeq 500$ m, within an $80 \times 80 \times 20$ km domain (from Klemp and Skamarock 2004).

5. Summary

In this paper, we have presented new time-splitting techniques for numerically integrating the nonhydrostatic equations in flux form. With this approach, the prognostic equations are cast in terms of variables that have conservation properties, while thermodynamic variables that have no direct conservation laws, such as temperature and pressure, are recovered from diagnostic relationships. These techniques permit the numerical conservation of mass and other first-order scalar quantities, which is an important attribute in atmospheric transport models.

We have developed the time-split integration procedures for two different vertical coordinates; the terrain-following height coordinate and the terrain-following hydrostatic pressure (mass) coordinate. For each system, we have analyzed the linear dispersion equation to identify the terms that need to be integrated on the small (acoustic) time steps and how those terms must be represented in time to achieve computational stability (see appendix). Numerical testing of these time-split procedures on a variety of idealized test cases confirm that the height- and mass-coordinate prototypes are robust over a wide range of scales, and that they produce nearly identical results. In addition, extensive real-time forecasting over the continental United States has confirmed that these two systems produce very comparable results, both on a case-by-case basis and statistically.

These tests suggest that both the height and mass vertical coordinates provide viable frameworks for the time-split integration of the nonhydrostatic equations. The mass coordinate, however, exhibits some beneficial characteristics that bear consideration in selecting the vertical coordinate. With the mass coordinate, a constant pressure upper surface allows the atmosphere to expand or contract vertically in response to heating and cooling, which allows a more realistic response to diabatic processes. In contrast, for the height coordinate with a rigid upper surface, heating can produce artificial pressure increases or mass removal (depending on the numerical implementation). While this differential behavior may not be significant for localized diabatic effects in deep atmospheric domains, it may be important for persistent large-scale forcing such as radiative heating. Since the upper surface in the mass coordinate can be defined as a material surface, this coordinate maintains its conservation properties with a broader range of upper boundary conditions (constant pressure, rigid lid, gravity wave radiation). The mass coordinate requires some additional computations to keep track of the moving coordinate surfaces (adding several percent to the computation time over the height-coordinate system for the dynamic portion of the code); however, the

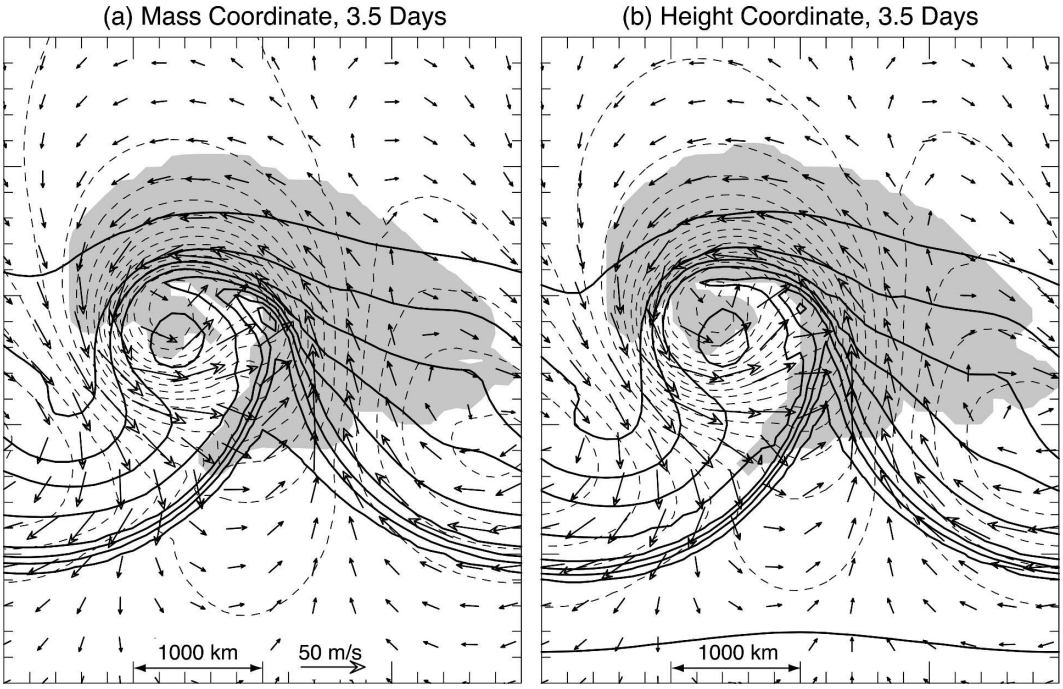

FIG. 3. Baroclinic wave in a channel for the (a) mass-coordinate and (b) height-coordinate simulations at 3.5 days, depicting the temperature (solid lines, CI = 4 K), cloud field (shaded), and horizontal wind vectors at $z = 150$, together with surface pressure (dashed lines, CI = 4 mb). The model grid is $\Delta x = \Delta y = 100$ km and $\Delta z \simeq 250$ m within a $4000 \times 6000 \times 16$ km domain.

mass coordinate allows simplification of the numerics for hydrostatic applications with a simple switch through which the code reverts to the traditional hydrostatic sigma system.

APPENDIX

Time Splitting for Acoustic and Gravity Waves

When choosing equations and a discretization for a split-explicit model, one must determine which terms in the governing equations are associated with the acoustic and (optionally) gravity wave modes that need to be included in the small time steps. Within the flux-form equations that do not use pressure as a prognostic variable, it is not clear, at first glance, which terms need to be included on the small time steps, and which small-step terms need to be handled implicitly to achieve an implicit discretization for vertically propagating acoustic modes.

To answer these questions, we examine the dispersion relation for the continuous and discrete systems, for the simplified case of two-dimensional flow with no mean wind (no advection), and for an isothermal atmosphere ($c^2 = \gamma R\overline{T} = $ constant) so that the linear system will have constant coefficients. In order of importance, we seek to:

1) determine, for the acoustic time-step scheme, which terms are responsible for the acoustic mode propagation, and to determine which terms to treat implicitly to accommodate vertical propagation;
2) assure that frequencies for the discrete system are real (imaginary frequencies result in exponential growth and lead to numerical instability), which requires that imaginary terms in the discrete dispersion equation cancel numerically; and
3) determine the differencing that provides consistent treatment of real terms in the discrete dispersion relation, such that terms that cancel in the continuous equation also cancel in the discretized equation.

a. Height-coordinate equations

In linearizing the equations expressed in the terrain-following height coordinate ζ, we define ζ in terms of mean dependent variables such that the vertical coordinate effectively reverts to height z. We then begin with the dry linear equations derived from (4)–(7):

$$\underset{U_{\Theta x}}{\partial_t U + c^2 \partial_x \tilde{\Theta}'} = 0, \tag{A1}$$

$$\underset{W_{\Theta z}}{\partial_t W} + c^2 \underset{W_{\Theta z}}{\partial_z \tilde{\Theta}'} + c^2 \underset{W_{\Theta z}}{\frac{N^2}{g}} \tilde{\Theta}' - g \underset{W_{\Theta B}}{\frac{R}{c_v}} \tilde{\Theta}' + \underset{W_{\rho B}}{g\rho'} = 0, \tag{A2}$$

$$\underset{R_{Ux}}{\partial_t \rho'} + \underset{R_{Ux}}{\partial_x U} + \underset{R_{Wz}}{\partial_z W} = 0, \quad \text{and} \tag{A3}$$

$$\underset{\Theta_{Ux}}{\partial_t \tilde{\Theta}'} + \underset{\Theta_{Wz}}{\partial_x U} + \underset{\Theta_{Wz}}{\partial_z W} + \underset{\Theta_{Wz}}{\frac{N^2}{g}} W = 0, \tag{A4}$$

where the variables are as described in section 2 with the prime notation designating perturbation quantities, and defining $\tilde{\Theta}' = \Theta'/\bar{\theta}$ to achieve a form in which all coefficients are independent of height. The notations below the terms in (A1)–(A4) are tags that will track where each term contributes to the discrete dispersion relation, and will be used to identify the discretization in time for the respective terms. Substituting the Fourier representation $\psi = \hat{\psi} \exp[i(kx + lz - \omega t)]$ for each of the variables in (A1)–(A4) then yields

$$\det \begin{vmatrix} \omega & 0 & 0 & -kc^2 \\ 0 & \omega & ig & -lc^2 + i\left(\dfrac{c^2N^2}{g} - g\dfrac{R}{c_v}\right) \\ -k & -l & \omega & 0 \\ -k & -l + i\dfrac{N^2}{g} & 0 & \omega \end{vmatrix} = 0.$$

Recognizing that the vertical wavenumber will have an imaginary part ($l = l_R + il_I$), the frequency equation becomes

$$\omega^4 - \left[\underset{U_{\Theta x}\Theta_{Ux}}{k^2} + \underset{W_{\Theta z}\Theta_{Wz}}{l_R^2} - \underset{\Theta_{Wz}}{\frac{N^2}{g}} \left(\underset{W_{\Theta z}}{\frac{N^2}{g}} - \underset{W\Theta B}{\frac{R}{c_v}} \frac{g}{c^2} \right) \right.$$

$$\left. - l_I \left(\underset{W_{\Theta z}\Theta_{Wz}}{l_I} - \beta \right) + il_R \left(\underset{W_{\Theta z}\Theta_{Wz}}{2l_I} - \beta \right) \right] c^2\omega^2$$

$$+ \underset{U_{\Theta x}}{kc^2} \left[\underset{R_{Ux}\Theta_{Wz}W_{\rho B}}{kN^2} + \underset{R_{Ux}\Theta_{Wz}W_{\rho B}}{igkl} - \underset{R_{Wz}\Theta_{Ux}W_{\rho B}}{igkl} \right] = 0, \tag{A5}$$

where

$$\beta = \underset{W_{\Theta z}\Theta_{Wz}}{\frac{N^2}{g}} - \underset{W_{\Theta B}\Theta_{Wz}}{\frac{R}{c_v}} \frac{g}{c^2} + \underset{W_{\Theta z}\Theta_{Wz}}{\frac{N^2}{g}} + \underset{R_{Wz}W_{\rho B}}{\frac{g}{c^2}}. \tag{A6}$$

In the dispersion relation (A5), the first three terms are the primary terms responsible for sound-wave propagation:

$$\omega^4 - (k^2 + l_R^2)c^2\omega^2 = 0. \tag{A7}$$

We want to handle the acoustic modes on the small time step, treating horizontally propagating terms explicitly using forward–backward differencing and the vertically propagating terms implicitly (as in Klemp and Wilhelmson 1978). Denoting terms handled explicitly on the small time steps using values at time τ as E^-, terms evaluated explicitly using values at $\tau + \Delta\tau$ as E^+, and terms represented implicitly as I, this treatment requires

$$U_{\Theta x} => E^-, \quad \Theta_{Ux} => E^+, \quad \text{and}$$
$$W_{\Theta z} <=> \Theta_{Wz} => I, \tag{A8}$$

where the notation => associates a particular term in the equations with a specific numerical representation in time, and <=> associates terms that must have the same time discretization.

Because ω must be real to maintain stability, the *igkl* terms in the dispersion relation (A5) must cancel exactly, which requires

$$R_{Ux}\Theta_{Wz} <=> R_{Wz}\Theta_{Ux}$$

and hence, given (A8)

$$R_{Ux} => E^+, \quad R_{Wz} => I. \tag{A9}$$

In addition, we recognize that for real frequencies, $l_I = \beta/2$, which removes the imaginary part of the coefficient of $c^2\omega^2$ in (A5).

With the time discretization specified as indicated in (A8) and (A9), the first two of the three objectives listed above are satisfied. The only terms remaining in (A1)–(A4) whose time discretizations have not yet been specified are the buoyancy terms [the last three terms in (A2) tagged by $W_{\Theta B}$ and $W_{\rho B}$]. While these terms are not important to the propagation of acoustic modes, they are fundamental contributors to the gravity wave modes. They could be evaluated on the large time steps and still maintain stability in the time-split integration. However with this approach, the large time step would be constrained by the gravity wave frequency (essentially the Brunt–Väisälä frequency N), and several terms that should cancel in the dispersion equation [the fourth and fifth terms in (A5) and the first two terms on the rhs of (A6)] will not exactly cancel in the discrete system [recognizing that $N^2/g = (R/c_v)(g/c^2)$ in the isothermal atmosphere]. These inconsistencies are avoided by evaluating the buoyancy terms on the small time step, which can be accommodated

with little additional computational cost. Thus, to satisfy the third objective and achieve numerical cancellation of the terms mentioned above, the buoyancy terms should be solved implicitly:

$$W_{\Theta B} <=> W_{\rho B} => I. \tag{A10}$$

With this treatment of the buoyancy terms, the discretized form of l_I from (A6) becomes

$$l_I = \frac{\beta}{2} = \frac{1}{2}\left(\frac{N^2}{g} + \frac{g}{c^2}\right) = -\frac{1}{2}\frac{\overline{\rho}_z}{\overline{\rho}}, \tag{A11}$$

which confirms that disturbances will amplify with height in proportion to the inverse square root of the mean density (as expected).

The time differencing indicated by (A8)–(A10) completes the specification for (A1)–(A4). The dispersion equation [(A5)] becomes

$$\omega^4 - \underbrace{\left(\underbrace{k^2}_{E^+E^-} + \underbrace{l_R^2}_{II} + \underbrace{\frac{\beta^2}{4}}_{II}\right)}_{E^+E^-II} c^2\omega^2 + k^2c^2N^2 = 0, \tag{A12}$$

which agrees with the analytic relationship. The time-discretized dispersion equation is then given by

$$\sin^4\frac{\omega\Delta\tau}{2} - \left[k^2 + \left(l_R^2 + \frac{\beta^2}{4}\right)\cos^2\frac{\omega\Delta\tau}{2}\right]c^2\sin^2\frac{\omega\Delta\tau}{2} + k^2c^2N^2\cos^2\frac{\omega\Delta\tau}{2} = 0, \tag{A13}$$

confirming that the equation remains second-order centered on the small time steps. This time-discretized form follows immediately from (A12) recognizing that ω is replaced by $(2/\Delta\tau)\sin(\omega\Delta\tau/2)$, terms designated by E^+ and E^- are multiplied by $\exp(-i\omega\Delta\tau/2)$ and $\exp(+i\omega\Delta\tau/2)$, respectively, and terms designated by I are multiplied by $\cos(\omega\Delta\tau/2)$.

The temporal discretization for the linear system is thus given by

$$\delta_\tau U + \frac{c^2}{\overline{\theta}}\partial_x\Theta'^\tau = 0, \tag{A14}$$

$$\delta_\tau W + \frac{c^2}{\overline{\theta}}\overline{\partial_z\Theta'}^\tau + \overline{g\rho'}^\tau - \frac{gR}{c_v\overline{\theta}}\overline{\Theta'}^\tau = 0, \tag{A15}$$

$$\delta_\tau\rho' + \partial_x U^{\tau+\Delta\tau} + \overline{\partial_z W}^\tau = 0, \quad \text{and} \tag{A16}$$

$$\delta_\tau\Theta' + \partial_x(\overline{\theta}U^{\tau+\Delta\tau}) + \overline{\partial_z(\overline{\theta}W)}^\tau = 0. \tag{A17}$$

The solution procedure for the small time steps is to advance the horizontal momentum equation first [(A14)], and then to advance the vertically implicit equations [(A15)–(A17)], given that the horizontal derivatives of $U^{\tau+\Delta\tau}$ in (A16) and (A17) can be evaluated after advancing (A14). The implicit solution requires solving a tridiagonal matrix for each grid column.

b. Mass-coordinate equations

For the mass-coordinate system, we also express the terrain-following vertical coordinate in terms of mean-state quantities [$\eta = (p_h - p_{ht})/\overline{\mu}$], such that η essentially reverts to the hydrostatic pressure vertical coordinate. In this coordinate, the flux-form variables (coupled with $\overline{\mu}$ = constant) are the same as the uncoupled variables, and thus the dry linear system (2D, no advection) based on (22)–(29) becomes

$$\partial_t u + \underbrace{\partial_x\tilde{p}'}_{u_{px}} + \underbrace{\partial_x\phi'}_{u_{\phi x}} = 0, \tag{A18}$$

$$\partial_t w - \underbrace{\frac{g}{\overline{\mu}\,\overline{\alpha}}\partial_\eta\tilde{p}'}_{w_{p\eta}} - \underbrace{\beta\tilde{p}'}_{w_{p\eta}} = 0, \tag{A19}$$

$$\partial_t\phi' - \underbrace{\tilde{\dot{\eta}}'}_{\phi_{\dot{\eta}}} - \underbrace{gw}_{\phi_w} = 0, \tag{A20}$$

$$\partial_t\tilde{\theta}' - \underbrace{\frac{N^2}{g^2}\tilde{\dot{\eta}}'}_{\theta_{\dot{\eta}}} = 0, \tag{A21}$$

together with the diagnostic constraints

$$\partial_x u + \frac{1}{\overline{\mu}\,\overline{\alpha}}\partial_\eta\tilde{\dot{\eta}}' + \frac{\beta}{g}\tilde{\dot{\eta}}' = 0, \quad \frac{1}{\overline{\mu}\,\overline{\alpha}}\partial_\eta\phi' = -\tilde{\alpha}', \quad \text{and}$$

$$\tilde{p}' = c^2(\tilde{\theta}' - \tilde{\alpha}'). \tag{A22}$$

Here, the perturbation variables have been scaled by defining $\tilde{p}' = \overline{\alpha}p'$, $\tilde{\dot{\eta}}' = \overline{\mu}\,\overline{\alpha}\dot{\eta}'$, $\tilde{\theta}' = \theta'/\overline{\theta}$, and $\tilde{\alpha}' = \alpha'/\overline{\alpha}$. Recognizing that $(1/\overline{\mu}\,\overline{\alpha})\partial_\eta = -(1/g)\partial_z$, with this scaling (A18)–(A22) will have constant coefficients for normal modes of the form $\psi = \hat{\psi}\exp[i(kx + lz - \omega t)]$. Also, we define $\beta \equiv \overline{\alpha}_z/\overline{\alpha}$ as in (A11).

Representing the variables in terms of these normal modes yields a determinant that can be evaluated to obtain the dispersion relation. Here, the three diagnostic relationships in (A22) are used to eliminate the variables $\tilde{p}'$, $\tilde{\alpha}'$, and $\tilde{\dot{\eta}}'$, resulting in a 4×4 determinant for the prognostic equations [(A18)–(A21)]:

$$\det\begin{vmatrix} \omega & 0 & -k\left(1 - \dfrac{ilc^2}{g}\right) & -kc^2 \\ 0 & \omega & \dfrac{ilc^2}{g}(l + i\beta) & -(l + i\beta)c^2 \\ -\dfrac{igk}{(l + i\beta)} & -ig & \omega & 0 \\ -\dfrac{ikN^2}{g(l + i\beta)} & 0 & 0 & \omega \end{vmatrix} = 0.$$

Evaluating this determinant produces the frequency equation

$$\omega^4 - k^2\left[\underset{\phi_{\dot\eta}}{\frac{1}{l+i\beta}}\left(\underset{u_{px}}{l} + i\underset{u_{\phi x}}{\frac{g}{c^2}}\right) + \underset{\theta_{\dot\eta}}{\frac{i}{l+i\beta}}\underset{u_{px}}{\frac{N^2}{g}}\right]c^2\omega^2 - \underset{\phi_w w_{p\eta}}{l(l+i\beta)c^2\omega^2} + \underset{\theta_{\dot\eta}\phi_w}{\frac{k^2N^2c^2}{l+i\beta}}\left[\left(\underset{u_{\phi x}}{1} - \underset{u_{px}}{\frac{ilc^2}{g}}\right)\underset{w_{p\eta}}{(l+i\beta)} + \underset{u_{px}}{\frac{ilc^2}{g}}\underset{w_{p\eta}}{(l+i\beta)}\right] = 0. \quad \text{(A23)}$$

Recalling (A7), we recognize that the second major term in (A23) is responsible for the horizontal sound-wave propagation and thus the u_{px}, $u_{\phi x}$, $\phi_{\dot\eta}$, and $\theta_{\dot\eta}$ terms in (A18)–(A21) must be included on the small time steps. For the frequency to be real (numerically stable), this term must be real; this is satisfied if

$$u_{px} <=> u_{\phi x} \quad \text{and} \quad \phi_{\dot\eta} <=> \theta_{\dot\eta}, \quad \text{(A24)}$$

in which case the expression in brackets reduces numerically to unity.

The third major term in (A23) represents the vertical sound-wave propagation; to treat these terms implicitly on the small time steps requires

$$w_{p\eta} <=> \phi_w => I. \quad \text{(A25)}$$

This term also defines the imaginary part of the vertical wavenumber ($l = l_R + il_I$) to be $l_I = -\beta/2$ for this term to be real. Notice that this value of l_I is the same as in (A11) for the height coordinate except opposite in sign. This sign difference occurs because in the height-coordinate analysis, the normal-mode variables have been coupled with density.

The last major term in (A23) is a fundamental contributor to the gravity wave modes. Although this term is not essential to the acoustic modes, it is formed from terms designated in (A24) and (A25) that are required for sound-wave propagation. Consequently, in this vertical coordinate, the terms governing the acoustic and gravity wave modes are intermingled to the extent that it does not appear feasible to evaluate any of the gravity wave terms on the large time steps, even if one desired to do so. With proper specification of the numerics, this final term in the discretized dispersion equation remains real and reduces to $k^2N^2c^2$. Using forward–backward time differencing for the horizontally propagating acoustic modes, this will be achieved provided

$$u_{px} => E^- \quad \text{and} \quad \phi_{\dot\eta} => E^+. \quad \text{(A26)}$$

Representing the time discretization of the small time step terms according to (A24)–(A26), the dispersion equation is now identical to (A12) and (A13), confirming again that the frequency remains real and the time differencing will be second-order centered.

For the linear system, the temporal discretization for terms integrated on the small time steps is thus represented by

$$\delta_\tau u + \overline{\alpha}\partial_x p'^\tau + \phi_x'^\tau = 0, \quad \text{(A27)}$$

$$\partial_x u^{\tau+\Delta\tau} + \partial_\eta \dot\eta'^{\tau+\Delta\tau} = 0, \quad \text{(A28)}$$

$$\delta_\tau \theta' + \overline{\theta}_\eta \dot\eta'^{\tau+\Delta\tau} = 0, \quad \text{(A29)}$$

$$\delta_\tau w - \frac{g}{\overline{\mu}}\overline{\partial_\eta p'}^\tau = 0, \quad \text{and} \quad \text{(A30)}$$

$$\delta_\tau \phi' + \overline{\phi}_\eta \dot\eta'^{\tau+\Delta\tau} - g\overline{w}^\tau = 0. \quad \text{(A31)}$$

These equations are integrated by first stepping forward the horizontal momentum equation [(A27)] and then obtaining $\dot\eta'$ at the new time level from the continuity equation in (A28). Equation (A29) can next be stepped forward to obtain θ at the new time level. Finally, (A30) and (A31) are advanced by solving a tridiagonal matrix for the vertically implicit portion of the equations, having replaced the p' term in (A30) by terms involving ϕ' and θ' by combining the last two equations in (A22) as discussed in section 3.

REFERENCES

Anthes, R. A., and T. T. Warner, 1978: Development of hydrodynamic models suitable for air pollution and other mesometeorological studies. *Mon. Wea. Rev.,* **106,** 1045–1078.

Arakawa, A., and V. R. Lamb, 1977: Computational design of the basic dynamical processes of the UCLA general circulation model. *Methods in Computational Physics,* Vol. 17, J. Chang, Ed., Academic Press, 173–265.

Bartello, P., and S. J. Thomas, 1996: The cost-effectiveness of semi-Lagrangian advection. *Mon. Wea. Rev.,* **124,** 2883–2897.

Byun, D. W., 1999: Dynamically consistent formulations in meteorological and air quality models for multiscale atmospheric studies. Part I: Governing equations in a generalized coordinate system. *J. Atmos. Sci.,* **56,** 3789–3807.

Chorin, A. J., 1967: A numerical method for solving incompressible viscous flow problems. *J. Comput. Phys.,* **2,** 12–26.

Clark, T. L., 1977: A small-scale dynamic model using a terrain-following coordinate transformation. *J. Comput. Phys.,* **24,** 186–215.

——, 1979: Numerical simulations with a three-dimensional cloud model: Lateral boundary condition experiments and multicellular severe storm simulations. *J. Atmos. Sci.,* **36,** 2191–2215.

Davies, T., A. Staniforth, N. Wood, and J. Thuburn, 2003: Validity of anelastic and other equation sets as inferred from normal-mode analysis. *Quart. J. Roy. Meteor. Soc.,* **129,** 2761–2775.

Doms, G., and U. Schättler, Eds., 1999: The nonhydrostatic limited-area model LM (Lokal Model) of DWD. Part I: Scien-

tific documentation. Deutscher Wetterdienst Rep. LM F90 1.35, 172 pp. [Available from Deutscher Wetterdienst, P.O. Box 100465, 63004 Offenbach, Germany.]

Droegemeier, K. K., and R. B. Wilhelmson, 1987: Numerical simulation of thunderstorm outflow dynamics. Part I: Outflow sensitivity experiments and turbulence dynamics. *J. Atmos. Sci.,* **44,** 1180–1210.

Dudhia, J., 1993: A nonhydrostatic version of the Penn State–NCAR Mesoscale Model: Validation tests and simulation of an Atlantic cyclone and cold front. *Mon. Wea. Rev.,* **121,** 1493–1513.

Durran, D. R., 1989: Improving the anelastic approximation. *J. Atmos. Sci.,* **46,** 1453–1461.

——, 1999: *Numerical Methods for Wave Equations in Geophysical Fluid Dynamics.* Springer-Verlag, 465 pp.

——, and J. B. Klemp, 1983: A compressible model for the simulation of moist mountain waves. *Mon. Wea. Rev.,* **111,** 2341–2361.

Dutton, J. A., 1976: *Dynamics of Atmospheric Motion*. Dover, 617 pp.

Hodur, R. M., 1997: The Naval Research Laboratory's Coupled Ocean/Atmosphere Mesoscale Prediction System (COAMPS). *Mon. Wea. Rev.,* **125,** 1414–1430.

Klemp, J. B., and R. B. Wilhelmson, 1978: The simulation of three-dimensional convective storm dynamics. *J. Atmos. Sci.,* **35,** 1070–1096.

——, and D. R. Durran, 1983: An upper boundary condition permitting internal gravity wave radiation in numerical mesoscale models. *Mon. Wea. Rev.,* **111,** 430–444.

——, and W. Skamarock, 2004: Model numerics for convective-storm simulation. *Atmospheric Turbulence and Mesoscale Meteorology: Scientific Research Inspired by Doug Lilly,* E. Federovich et al., Eds., Cambridge University Press, 117–137.

Laprise, R., 1992: The Euler equations of motion with hydrostatic pressure as an independent variable. *Mon. Wea. Rev.,* **120,** 197–207.

Lipps, F. B., and R. S. Hemler, 1982: A scale analysis of deep moist convection and some related numerical calculations. *J. Atmos. Sci.,* **39,** 2192–2210.

Madala, R. V., 1981: Efficient time integration schemes for atmosphere and ocean models. *Finite-Difference Techniques for Vectorized Fluid Dynamics Calculations,* D. L. Book, Ed., Springer-Verlag, 56–70.

Ogura, Y., and N. A. Phillips, 1962: Scale analysis of deep and shallow convection in the atmosphere. *J. Atmos. Sci.,* **19,** 173–179.

Ooyama, K. V., 1990: A thermodynamic foundation for modeling the moist atmosphere. *J. Atmos. Sci.,* **47,** 2580–2596.

Pinty, J.-P., R. Benoit, E. Richard, and R. Laprise, 1995: Simple tests of a semi-implicit semi-Lagrangian model on 2D mountain wave problems. *Mon. Wea. Rev.,* **123,** 3042–3058.

Rotunno, R., W. C. Skamarock, and C. Snyder, 1994: An analysis of frontogenesis in numerical simulations of baroclinic waves. *J. Atmos. Sci.,* **51,** 3373–3398.

Saito, K., and Coauthors, 2006: The operational JMA nonhydrostatic mesoscale model. *Mon. Wea. Rev.,* **134,** 1266–1298.

Skamarock, W. C., and J. B. Klemp, 1992: The stability of time-split numerical methods for the hydrostatic and the nonhydrostatic elastic equations. *Mon. Wea. Rev.,* **120,** 2109–2127.

——, ——, and J. Dudhia, 2001: Prototypes for the WRF (Weather Research and Forecast) model. Preprints, *Ninth Conf. on Mesoscale Processes,* Fort Lauderdale, FL, Amer. Meteor. Soc., CD-ROM, J1.5.

——, ——, ——, D. O. Gill, D. M. Barker, W. Wang, and J. G. Powers, 2005: A description of the Advanced Research WRF Version 2. NCAR Tech. Note NCAR/TN-468+STR, 88 pp.

Smolarkiewicz, P. K., L. G. Margolin, and A. A. Wyszogrodzki, 2001: A class of nonhydrostatic global models. *J. Atmos. Sci.,* **58,** 349–364.

Staniforth, A., and J. Côté, 1991: Semi-Lagrangian integration schemes for atmospheric models—A review. *Mon. Wea. Rev.,* **119,** 2206–2223.

Straka, J., R. B. Wilhelmson, L. J. Wicker, J. R. Anderson, and K. K. Droegemeier, 1993: Numerical solutions of a nonlinear density current: A benchmark solution and comparisons. *Int. J. Numer. Methods Fluids,* **17,** 1–22.

Tanguay, M., A. Robert, and R. Laprise, 1990: A semi-implicit semi-Lagrangian fully compressible regional forecast model. *Mon. Wea. Rev.,* **118,** 1970–1980.

Tapp, M. C., and P. W. White, 1976: A non-hydrostatic mesoscale model. *Quart. J. Roy. Meteor. Soc.,* **102,** 277–296.

Thomas, S., C. Girard, G. Doms, and U. Schättler, 2000: Semi-implicit scheme for the DWD Lokal-Modell. *Meteor. Atmos. Phys.,* **73,** 105–125.

Tripoli, G. J., 1992: A nonhydrostatic mesoscale model designed to simulate scale interaction. *Mon. Wea. Rev.,* **120,** 1342–1359.

——, and W. R. Cotton, 1982: The Colorado State University three-dimensional cloud/mesoscale model. Part I: General theoretical framework and sensitivity experiments. *J. Rech. Atmos.,* **16,** 185–220.

Weisman, M. L., and J. B. Klemp, 1984: Characteristics of isolated convective storms. *Mesoscale Meteorology and Forecasting,* P. S. Ray, Ed., Amer. Meteor. Soc., 331–358.

Wicker, L. J., and R. B. Wilhelmson, 1995: Simulation and analysis of tornado development and decay within a three-dimensional supercell thunderstorm. *J. Atmos. Sci.,* **52,** 2675–2703.

——, and W. C. Skamarock, 1998: A time-splitting scheme for the elastic equations incorporating second-order Runge–Kutta time differencing. *Mon. Wea. Rev.,* **126,** 1992–1999.

——, and ——, 2002: Time-splitting methods for elastic models using forward time schemes. *Mon. Wea. Rev.,* **130,** 2088–2097.

Wilhelmson, R. B., and Y. Ogura, 1972: The pressure perturbation and the numerical modeling of a cloud. *J. Atmos. Sci.,* **29,** 1295–1307.

Xue, M., K. K. Droegemeier, and V. Wong, 2000: The Advanced Regional Prediction System (ARPS)—A multi-scale nonhydrostatic atmospheric simulation and prediction model. Part I: Model dynamics and verification. *Meteor. Atmos. Phys.,* **75,** 161–193.

Yeh, K.-S., J. Côté, S. Gravel, A. Méthot, A. Patoine, M. Roch, and A. Staniforth, 2002: The CMC–MRB Global Environmental Multiscale (GEM) model. Part III: Nonhydrostatic formulation. *Mon. Wea. Rev.,* **130,** 339–356.